

Fairy Lights in Femtoseconds: Aerial and Volumetric Graphics Rendered by Focused Femtosecond Laser Combined with Computational Holographic Fields

YOICHI OCHIAI

University of Tsukuba

KOTA KUMAGAI

Utsunomiya University

TAKAYUKI HOSHI

Nagoya Institute of Technology

JUN REKIMOTO

The University of Tokyo

and

SATOSHI HASEGAWA and YOSHIO HAYASAKI

Utsunomiya University

We present a method of rendering aerial and volumetric graphics using femtosecond lasers. A high-intensity laser excites physical matter to emit light at an arbitrary three-dimensional position. Popular applications can thus be explored, especially because plasma induced by a femtosecond laser is less harmful than that generated by a nanosecond laser. There are two methods of rendering graphics with a femtosecond laser in air: producing holograms using spatial light modulation technology and scanning of a laser beam by a galvano mirror. The holograms and workspace of the system proposed here occupy a volume of up to 1 cm^3 ; however, this size is scalable depending on the optical devices and their setup. This article provides details of the principles, system setup, and experimental evaluation, and discusses the scalability, design space, and applications of this system. We tested two laser sources: an adjustable (30–100fs) laser that projects up to 1,000 pulses/s at an energy of up to 7mJ/pulse and a 269fs laser that projects up to 200,000 pulses/s at an energy of up to $50 \mu\text{J}$ /pulse. We confirmed that the spatiotemporal resolution of volumetric displays implemented using these

laser sources is 4,000 and 200,000 dots/s, respectively. Although we focus on laser-induced plasma in air, the discussion presented here is also applicable to other rendering principles such as fluorescence and microbubbles in solid or liquid materials.

CCS Concepts: • **Hardware** → **Emerging optical and photonic technologies**

Additional Key Words and Phrases: Volumetric display, laser plasma, femtosecond laser, aerial interaction, touchable aerial images

ACM Reference Format:

Yoichi Ochiai, Kota Kumagai, Takayuki Hoshi, Jun Rekimoto, Satoshi Hasegawa, and Yoshio Hayasaki. 2016. Fairy lights in femtoseconds: Aerial and volumetric graphics rendered by focused femtosecond laser combined with computational holographic fields. *ACM Trans. Graph.* 35, 2, Article 17 (February 2016), 14 pages.

DOI: <http://dx.doi.org/10.1145/2850414>

Y. Ochiai and K. Kumagai are joint first authors.

Authors' addresses: Y. Ochiai, 1-2 Kasuga, Tsukuba-shi, Ibaraki, 305-8550 Japan; email: wizard@slis.tsukuba.ac.jp; K. Kumagai, S. Hasegawa, and Y. Hayasaki, 7-1-2 Yoto, Utsunomiya-shi, Tochigi, 321-8585 Japan; emails: {[kumagai_k](mailto:kumagai_k@opt.utsunomiya-u.ac.jp), [hasegawa_s](mailto:hasegawa_s@opt.utsunomiya-u.ac.jp), [hayasaki](mailto:hayasaki@opt.utsunomiya-u.ac.jp)}@opt.utsunomiya-u.ac.jp; T. Hoshi, Gokisocho, Showa-ku, Nagoyashi, Aichi, 466-855 Japan; email: star@nitech.ac.jp; J. Rekimoto, 7-3-1 Hongo, Bunkyo-ku, Tokyo, 113-0033 Japan; email: rekimoto@acm.org.

Permission to make digital or hard copies of part or all of this work for personal or classroom use is granted without fee provided that copies are not made or distributed for profit or commercial advantage and that copies show this notice on the first page or initial screen of a display along with the full citation. Copyrights for components of this work owned by others than ACM must be honored. Abstracting with credit is permitted. To copy otherwise, to republish, to post on servers, to redistribute to lists, or to use any component of this work in other works requires prior specific permission and/or a fee. Permissions may be requested from Publications Dept., ACM, Inc., 2 Penn Plaza, Suite 701, New York, NY 10121-0701 USA, fax +1 (212) 869-0481, or permissions@acm.org.

© 2016 ACM 0730-0301/2016/02-ART17 \$15.00

DOI: <http://dx.doi.org/10.1145/2850414>

1. INTRODUCTION

Three-dimensional (3D) displays have attracted great attention over the past 5 decades. Virtual 3D objects were originally displayed with a head-mounted display in Sutherland [1968]. Since then, continuous efforts have been made to explore 3D displays that have planar surfaces, and several methods have been developed to provide stereopsis for binocular vision [Benzie et al. 2007]. The technologies that employ glasses to achieve this are based on anaglyphs, time division, and polarization. On the other hand, those technologies that do not rely on glasses are based on a parallax barrier and lenticular lens array [Masia et al. 2013]. Although these methods can offer effective 3D images, they require calculation and generation of precise images for multiple viewpoints, and users have to stay within a limited view angle.

A different approach to realizing advanced 3D displays uses a physical 3D space instead of a planar surface to render graphics and forms a visual representation of an object in three physical dimensions, as opposed to the planar image of traditional screens

	Non position control	Position control
Reflection	Mechanical motion of mirror or screen [Paker] [Jones] [Favalora] [Karnik]	Screens deformed by linear actuators [Iwata] [Follmer] Soap film deformed by focused ultrasound [Ochiai] Small particles by acoustic levitation [Ochiai]
	Fog [Rakkolainen] [Lee]	
	Water drops [Eitoku] [Barnum]	
	Liquid crystal shutters [Sullivan]	
	Photochromic materials [Hashida]	
	Floating small particles [Perlin]	
Emission	Launched particles [Matoba]	Moved optical devices [Jansson] Fluorescence voxels [Macfarlane] LEDs on linear actuator [Poupyrev] Laser plasma [Kimura] This study
	Cubic array of LEDs [Clar]	
	3D fabricated optical fibers [Willis] [Pereira]	

Fig. 1. A map of related work divided into four categories regarding to non-position-control/position control and reflection/emission. This study falls into the position-control and emission category.

that simulate depth through various visual effects [Masia et al. 2013]. These 3D displays, which are called volumetric displays, allow users to view the displayed images from any angle. Volumetric displays arrange “voxels” in a 3D space. They are divided into four categories: nonposition-control/position-control and reflection/emission (Figure 1). Note that some of them are not 3D but 2.5D, and position control in 2.5D produces surface deformation. In this study, we focus on laser-induced plasma, which is in the position-control emission category.

Laser-induced plasma has the following advantages. First, it does not require special materials arranged and suspended in air to emit light. Second, it does not require wires and structures that possibly obstruct the line of sight because power is transmitted wirelessly. Third, the laser can be precisely controlled owing to progress in optical technologies.

We envision a laser-induced plasma technology with general applications for public use. If laser-induced plasma aerial images were made available, many useful applications such as augmented reality (AR), aerial user interfaces, and volumetric images could be produced (Figure 2). This would be a highly effective display for the expression of 3D information.

Volumetric expression has considerable merit because the content scale corresponds to that of the human body; therefore, this technology could be usefully applied to wearable materials and spatial user interactions. Further, laser focusing technology adds an additional dimension to conventional projection technologies, which offer surface mapping, whereas laser focusing technology is capable of volumetric mapping. Thus, this technology can be effectively used in real-world-oriented user interfaces.

Plasma-based 3D displays were previously developed using a nanosecond laser [Kimura et al. 2006] and femtosecond (100fs) laser [Saito et al. 2008]. Although these studies of laser-plasma graphics were innovative, they did not provide the details of the principles and technologies, and users were not allowed to touch the rendered graphics. Our motivation is to provide further discussion of this laser-plasma graphics technology and to expand the achievements of earlier work by enabling users to touch the rendered graphics.

In this study, we use femtosecond lasers with pulse durations of 30–100fs and 269fs. The plasma thus generated is less harmful than that obtained using nanosecond lasers, so the system can be

incorporated into everyday life. The design space and possible application scenarios of the plasma-based 3D display are discussed. In addition, we use an optical device called a spatial light modulator (SLM) to modify the phase of light rays and produce various spatial distributions of light based on interference.

The primary contribution of this article is the production by an ultrashort pulse duration laser of in-air SLM-based laser-plasma graphics that enable physical contact and interaction (Figure 3). In addition, the principles are theoretically described, the characteristics of this technology are experimentally examined, and the applications and scalability are discussed.

The rest of this article is organized as follows. First, we describe the principles and design parameters of femtosecond-laser-based volumetric displays. We explore a less harmful, high-resolution, adaptable laser-based volumetric display using a femtosecond laser and an SLM. Second, we introduce the setup we designed. Third, we give examples of applications. Finally, we conduct experiments on the generation and control of lasers and their damage to the skin. We also discuss the system’s limitations and estimate its scalability. We believe that this study fills gaps in the design space of plasma-based 3D displays that were left unresolved by previous studies.

2. RELATED WORK

2.1 Volumetric Displays

2.1.1 Non-Position-Control Types. Reflection: In this category, the work space is filled with small objects of a material that can passively reflect projected or environmental light. Three-dimensional displays based on mechanical motion of a mirror or screen are discussed in Parker [1948]. A spinning mirror is used with a high-speed projector in Jones et al. [2007], where different images are projected onto the mirror according to its azimuthal angle to express the 360° light field of an object. Similarly, images are projected onto a rotating screen [Favalora et al. 2002] and a rotating diffuser plate [Karnik et al. 2011]. The systems proposed in Rakkolainen et al. [2005a] and Lee et al. [2009] use fog as the reflecting material. A thin layer of fog is generated, and images are projected onto it. In Eitoku et al. [2006], falling water drops are utilized as a screen. Because of their lens-like properties, the water drops deliver projected images to users’ eyes. Subsequently, multi-layer water-drop screens were implemented [Barnum et al. 2010], and different images were projected onto different layers by synchronizing the projector with the water valves. In DepthCube [Sullivan 2004], a multilayered liquid crystal shutter is illuminated by a high-speed projector. Photochromic materials are used in Hashida et al. [2011] to form a volumetric and multicolor display controlled by an ultraviolet projector. In Holodust [Perlin and HAN 2006], small floating particles are illuminated by lasers. Small particles are launched into the air and illuminated by a projector in Matoba et al. [2012].

Emission: In this category, objects occupying the work space actively emit light to show images. Clar [2008] created a 3D cubic array of light-emitting diodes (LEDs). In this setup, the LEDs are supported by a framework, and their relative positions (i.e., voxel locations) are fixed. Fabrication-type 3D volume displays are currently being explored [Willis et al. 2012]. Three-dimensional printed objects with embedded light paths can display information when the objects are placed on a flat display. As the objects become more complex, the light paths also become complex, which makes it difficult to design the object to be printed. Pereira et al. [2014] solved this problem by algorithmically computing the arrangement

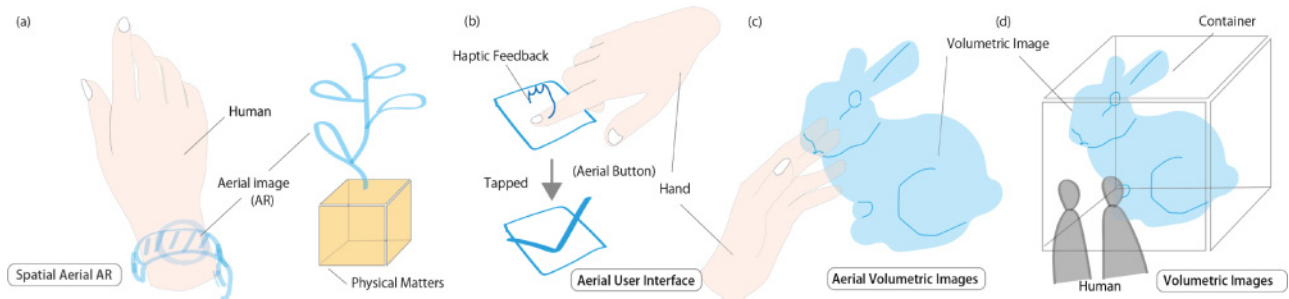


Fig. 2. These figures show the example applications of proposed laser-based graphics technology. (a) Images superposed on a hand and a box. (b) Floating button with haptic feedback. (c and d) Volumetric images rendered in open and closed areas.

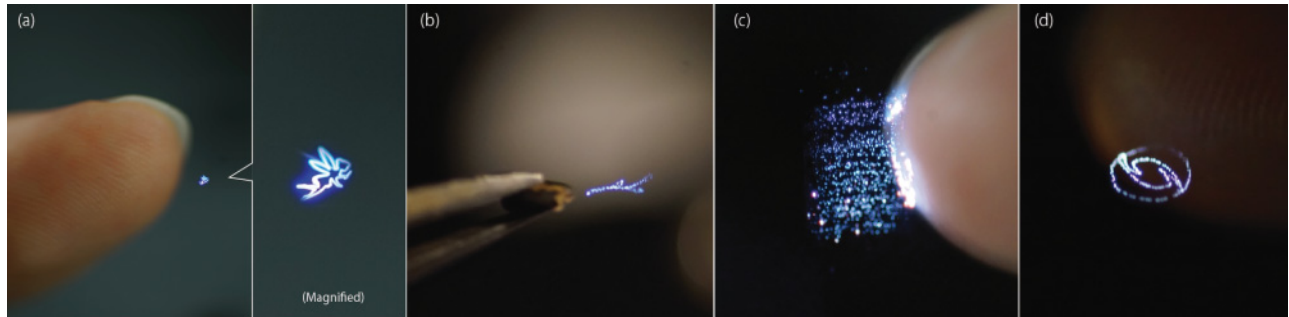


Fig. 3. Application images of Fairy Lights in Femtoseconds, aerial and volumetric graphics in air rendered by femtosecond lasers. (a) A “fairy” flying in front of a finger. (b) A “sprout” coming out from a seed. (c) Interference between a point cloud and a finger. (d) The SIGGRAPH logo.

of the light paths so that their endings form a desired surface shape, such as that of a face.

2.1.2 Position-Control Types. Reflection: In this category, the positions of reflection objects are controlled to render graphics. Studies focusing on controlling the surface shape of a screen or display have also been pursued. For example, the surface shape of the deformable screen in Project FEELEX [Iwata et al. 2001] is changed by linear actuators. The deformable screen in Form [Follmer et al. 2013] not only displays images but also interacts with objects. Ochiai et al. [2013] used focused ultrasound to deform a soap film, without making contact, to show a bump on it. Pixie Dust [Ochiai et al. 2014] is a floating display consisting of small particles that are suspended and moved by means of acoustic levitation.

Emission: Light sources are moved to realize 3D displays in this category. This type of volumetric display was originally reported in Jansson and Berlin [1979]. Many types of volumetric displays have been explored for 35 years. Grossman and Balakrishnan [2006] surveyed this area well. Macfarlane [1994] proposed a voxel-based spatial display. LUMEN [Poupyrev et al. 2004] consists of LEDs attached to linear actuators and shows information in the form of red-green-blue and height variations. Laser plasma, which is free from physical support and connections, is used as a light source in Kimura et al. [2006]. We also work with this technology to use this advantage.

2.2 Laser-Based Volumetric Displays

As mentioned above, laser-plasma 3D displays are categorized as position-control emission-type 3D displays. Voxels in air are generated by high-intensity laser pulses, which are realized by shortening

the pulse duration (e.g., to nanoseconds or shorter) under a limited time-averaged power.

The basic concept was demonstrated using a nanosecond laser in Kimura et al. [2006], where the rendering speed was 100 dots/s. The color of the voxels was bluish white because of plasma emission. Later, 1,000 dots/s was achieved [Saito et al. 2008], and rendering algorithms for a point cloud were discussed in Ishikawa and Saito [2008a, 2008b]. A femtosecond (100fs) laser was used there, but this information on the pulse duration appeared only on a Japanese website.¹ Although these studies of laser-plasma graphics were innovative, the published papers did not provide detailed discussions of the light emission, design space, scalability, and so on. We discuss these issues in this article and demonstrate complete laser-based graphics in air from principles to applications.

Laser-based 3D displays in materials other than air were also demonstrated. An in-water type² of laser-based volumetric display was developed in Kimura et al. [2011] and achieved 50,000 dots/s. Although no detailed principle was provided, we infer that this in-water type is based not on laser plasma but on laser-induced microbubbles. The dots of green light generated by a green laser can be explained by diffusion of the incident laser by the microbubbles. Fluorescent materials were used in Soltan et al. [1992], Downing et al. [1996], and Hasegawa and Hayasaki [2013]. The pulse peak intensity required for microbubble- and fluorescence-based rendering is experimentally confirmed in Section 5.3. This method offers

¹http://www.aist.go.jp/aist_j/press_release/pr2007/pr20070710/pr20070710.html (in Japanese) (last accessed June 17, 2015).

²<http://www.diginfo.tv/v/11-0231-r-en.php> (last accessed June 17, 2015).

Table I. Comparison between the Previous and This Study

	Kimura 2006	Saito 2008	This study
Medium	Air	Air	Air
Laser	Nanosecond	Femtosecond 100fs	Femtosecond A: 30-100fs, 2mJ B: 269fs, 50μJ
Dot/sec	100	1,000	A: 1,000 B: 200,000
Hologram	No	No	Yes LCOS-SLM or LCSLM
Interaction	No	No	Yes
Touch	No	No	Yes

a higher rendering speed than plasma-based rendering so that not a set of lines but a surface can be represented [Ishikawa et al. 2011].

2.3 Aerial Interaction

Volumetric, aerial, and/or 3D displays can usually interact with users' hands. For example, users can directly interact with graphics rendered on a thin layer of fog [Rakkolainen et al. 2005b]. Touchable Holography [Hoshi et al. 2009] and RePro3D [Yoshida et al. 2010] show 2D and 3D images in air, respectively, and also provide haptic feedback. Small particles are acoustically levitated in Ochiai et al. [2014], and users can touch them. ZeroN [Lee et al. 2011], although it is a tangible system rather than a graphic system, magnetically levitates a sphere, and users can touch and also handle it.

There are two necessary conditions for aerial interaction with volumetric displays: They should be safe and accessible. The previous works [Kimura et al. 2006; Saito et al. 2008] did not satisfy these conditions. The in-air type [Kimura et al. 2006] is harmful to users' hands because of the high laser power, and the in-water type [Kimura et al. 2011] renders images in a transparent container filled with water. In this article, we attempt to demonstrate a less harmful and touchable laser-based volumetric display.

2.4 Purpose of this Study

Conventional studies have encountered two problems in the development of a volumetric display: how to suspend and emit voxels. The application of laser plasma technology to a volumetric display overcomes these two issues because laser plasma generates an emission point at an arbitrary position in a 3D space. In addition, studies of previous laser volumetric displays have not sufficiently discussed the theoretical principles and scalability.

This study focuses on a system for rendering volumetric graphics in air using a femtosecond laser. Because our system uses an ultrashort-pulse laser and an SLM, we can explore touch interaction and computer-generated holograms (Table I). These explorations and evaluations are useful for discussing the scalability and application space of a plasma-based volumetric display using a high-intensity laser for general, widespread application.

3. PRINCIPLES

In this section, we show how to generate light spots in air using lasers.

3.1 Laser-Induced Light Spot

There are three types of laser-induced effects that produce light spots: Fluorescence in special materials, cavitation in fluids, and plasma in air. The required instantaneous power for these effects is quite different. In this study, we focus on the third effect (Figure 4), which requires the most power.

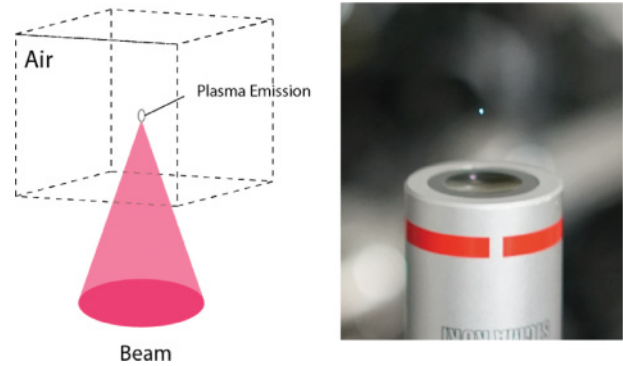


Fig. 4. Laser plasma induced by focused femtosecond laser.

Plasma is produced by tunnel ionization, which predominantly occurs when the laser intensity is greater than 10^{14}W/cm^2 [Keldysh 1965]. The potential well of a molecule or atom is deformed by the electric field of the high-intensity laser to have a potential barrier; then, an electron has the opportunity to leave the atom (i.e., ionization of the atom is possible) as a result of the tunnel effect. It is known that a higher laser intensity leads to a higher tunnel ionization probability; that is, more electrons are ionized [Ammosov et al. 1986]. The ionized electron is recombined with the atom after a half-cycle, and a photon is emitted. This effect is called *laser breakdown*. The emitted light looks bluish white.

3.2 Laser Filamentation

An emission dot generated by a high-intensity laser has a tail along the propagation direction. This tail is generated as the self-focusing behavior due to the optical Kerr effect competes with the natural diffraction of the laser beam; however, this effect is undesirable when rendering 3D graphics in air. Practically, this effect is invisible to the human eye because the light from the focal point is much brighter, but it might be taken into consideration in some special cases.

3.3 Voxel Sizes

We assume that the size of an emission dot (i.e., a voxel) is equal to the size of the focal point of the laser. The focal point is usually an oval that has two diameters. One is the diameter perpendicular to the laser beam, w_f , which is the diffraction limit and is determined by the original beam width a , focal length r , and wavelength λ such that

$$w_f = 2\lambda \frac{r}{a}. \quad (1)$$

The other is the diameter along the laser beam, w_d , which is geometrically obtained from the relationship $a : w_f = r : \frac{w_d}{2}$, such that

$$w_d = 4\lambda \left(\frac{r}{a}\right)^2. \quad (2)$$

3.4 Computational Phase Modulation

The use of SLMs is one method of rendering holograms. An SLM generally has an array of computer-controlled pixels that modulate a laser beam's intensities, phases, or both. This optical device is used in, for example, laser processing to generate an arbitrary laser pattern [Hayasaki et al. 2005].

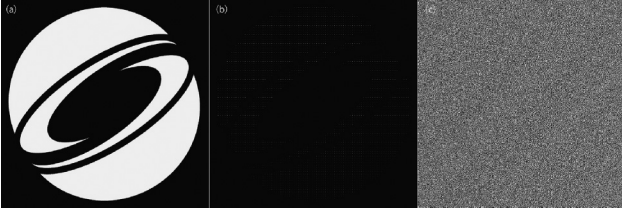


Fig. 5. Example of a computer-generated hologram (CGH). (a) An original image, (b) a converted spot-array image of the original image, and (c) a CGH to be displayed on the SLM.

A liquid crystal SLM (LCSLM), which contains a nematic liquid crystal layer, is used in this study. The molecule directions within this layer are controlled by electrodes, i.e., pixels, and the phase of the light ray reflected by each pixel is modulated according to the direction of the liquid crystal molecule. In other words, this device acts as an optical phased array.

The spatial phase control of light enables control of the focusing position along both the lateral (XY) and axial (Z) directions. The complex amplitude (CA) of the reconstruction from the computer-generated hologram (CGH) U_r is given by the Fourier transform of that of a designed CGH pattern U_h :

$$\begin{aligned} U_r(v_x, v_y) &= \iint U_h(x, y) \exp[-i2\pi(xv_x + yv_y)] dx dy \\ &= a_r(v_x, v_y) \exp[i\phi_r(v_x, v_y)] \end{aligned} \quad (3)$$

$$U_h(x, y) = a_h(x, y) \exp[i\phi_h(x, y)], \quad (4)$$

where a_h and ϕ_h are the amplitude and phase of the hologram plane displayed on the SLM, respectively. In the experiment, a_h is constant because the light irradiating the CGH is considered to be a plane wave with a uniform intensity distribution. ϕ_h is designed using the optimal rotation angle (ORA) algorithm [Bengtsson 1994]. On the other hand, a_r and ϕ_r are the amplitude and phase of the reconstruction plane, respectively. The spatial intensity distribution of the reconstruction is actually observed as $|U_r|^2 = a_r^2$.

To control the focusing position along the lateral (XY) direction, the CGH is designed on the basis of a superposition of the CAs of blazed gratings with various azimuth angles. If the reconstruction has N -multiple focusing spots, the CGH includes N -blazed gratings. To control the focusing position along the axial (Z) direction, a phase Fresnel lens pattern $\phi_p(x, y) = k \frac{x^2 + y^2}{2f}$ with a focal length f is simply added to ϕ_h , where $k = \frac{2\pi}{\lambda}$ is a wave number. In this case, the spatial resolution of the SLM determines the minimum focal length, according to the theory discussed in Section 3.3.

The ORA method is an optimization algorithm for obtaining the reconstruction of a CGH composed of a spot array with a uniform intensity (Figure 5). It is based on the addition of an adequate phase variation calculated by an iterative optimization process to the CGH. In the i -th iterative process, the amplitude a_h and phase $\phi_h^{(i)}$ at a pixel h on the CGH plane and the CA $U_r^{(i)}$ at a pixel r corresponding to the focusing position on the reconstruction plane are described computationally as follows:

$$\begin{aligned} U_r^{(i)} &= \omega_r^{(i)} \sum_h u_{hr}^{(i)} \\ &= \omega_r^{(i)} \sum_h a_h \exp[i(\phi_{hr} + \phi_h^{(i)})], \end{aligned} \quad (5)$$

where u_{hr} is the CA contributed from pixel h on the CGH plane to pixel r on the reconstruction plane, ϕ_{hr} is the phase contributed by light propagation from pixel h to pixel r , and $\omega_r^{(i)}$ is a weight coefficient that controls the light intensity at pixel r . To maximize the sum of the light intensity $\sum_r |U_r^{(i)}|^2$ at each pixel r , the phase variation $\Delta\phi_h^{(i)}$ added to $\phi_h^{(i)}$ at pixel h is calculated using the following equations.

$$\Delta\phi_h^{(i)} = \tan^{-1} \left(\frac{S_2}{S_1} \right), \quad (6)$$

$$S_1 = \sum_r \omega_r^{(i)} a_h \cos(\phi_r - \phi_{hr} - \phi_h^{(i)}), \quad (7)$$

$$S_2 = \sum_r \omega_r^{(i)} a_h \sin(\phi_r - \phi_{hr} - \phi_h^{(i)}), \quad (8)$$

where ω_r is the phase at pixel r on the reconstruction plane. The phase of the CGH, $\phi_h^{(i)}$, is updated by the calculated $\Delta\phi_h^{(i)}$ as follows.

$$\phi_h^{(i)} = \phi_h^{(i-1)} + \Delta\phi_h^{(i)}. \quad (9)$$

Furthermore, $\omega_r^{(i)}$ is also updated according to the light intensity of the reconstruction obtained by the Fourier transform of Equation (9) in order to control the light intensity at pixel r on the reconstruction plane.

$$\omega_r^{(i)} = \omega_r^{(i-1)} \left(\frac{I_r^{(d)}}{I_r^{(i)}} \right)^\alpha, \quad (10)$$

where $I_r^{(i)} = |U_r^{(i)}|^2$ is the light intensity at pixel r on the reconstruction plane in the i -th iterative process, $I_r^{(d)}$ is the desired light intensity, and α is a constant. The phase variation $\Delta\phi_h^{(i)}$ is optimized by the above iterative process (Equations (6)–(10)) until $I_r^{(i)}$ is nearly equal to $I_r^{(d)}$. Consequently, the ORA method allows us to design a high-quality CGH.

3.5 Positioning of Graphics

The galvano mirror used in this study covers an area of $10 \times 10 \text{ mm}^2$. Further, the SLM also renders graphics within approximately the same area. This means that we have two options for placing a point at an intended position: leading a laser there using the galvano mirrors or modifying the spatial distribution of the laser using the SLM. The conditions and/or response times of these devices determine which is suitable.

The theoretical rendering limit is 33 dots/s for 30 frames/s (fps) because the femtosecond laser is pulsed at a frequency of 1kHz. The SLM is used to render additional dots in a single frame, whereas the galvano mirror is used primarily for positioning the rendered holograms.

3.6 Spatiotemporal Resolution

The number of dots per frame (dpf) must be evaluated for laser-based volumetric displays. We now assume that the dots are displayed in darkness; therefore, the minimum required power for each dot is equal to the laser breakdown threshold E_{lbd} . The total output power E_{tot} is divided among the dots by the SLM. The number of dots per laser pulse, N_{dot} , is expressed as

$$N_{dot} = \frac{E_{tot}}{E_{lbd}}. \quad (11)$$

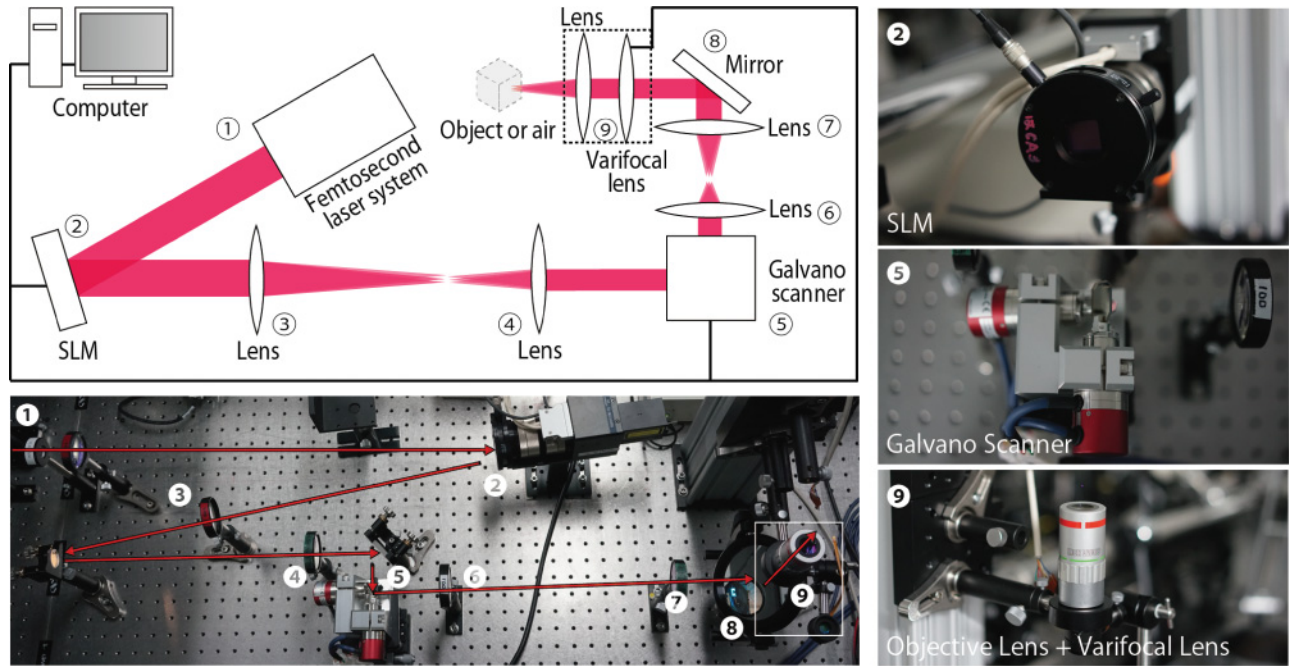


Fig. 6. Setup of our light circuit. The host computer controls (2) the SLM for hologram generation, (5) the galvano scanner for XY control, and (9) the varifocal lens for Z control.

The number of dots per frame is determined by N_{dot} , the repeat frequency F_{rep} of the laser pulses, and the frame time T_f , which is determined on the basis of the persistence of human vision. Hence,

$$dpf = N_{dot} \times F_{rep} \times T_f. \quad (12)$$

For example, if $N_{dot} = 100$, $F_{rep} = 1\text{kHz}$, and $T_f = 100\text{ms}$, an animation of 10,000dpf is played in 10fps. Note that, in practice, the number of dots per frame is determined by the bottleneck produced by the time response of the galvano mirrors and/or the SLM, instead of by F_{rep} .

4. IMPLEMENTATION

In this section, we describe our system implementation. First, we present an overview of our system. Next, we describe our light source, optical circuit (i.e., arrangement of optical devices), 3D scanning system, SLM, and control system.

4.1 Overview

Figure 6 shows the system configuration of our basic setup. This system aims to produce a simultaneous, multipoint volumetric display. It consists of a femtosecond laser source, an XYZ scanner (galvano scanner plus varifocal lens), and a liquid crystal on silicon SLM (LCOS-SLM) displaying a CGH for simultaneously addressed voxels. Our system was tested and investigated at 20.5°C. The atmosphere was ordinary air (80% N_2 and 20% O_2).

The setup was tested using two light sources (A and B), the specifications of which are given below. We primarily used a femtosecond laser source developed by Coherent Co., Ltd., which has a center wavelength of 800nm, repetition frequency of 1 kHz, and pulse energy in the 1mJ to 2mJ range. The specifications of the laser sources are shown in Table II. Figure 7 shows examples of results for our system in air.

Table II. Specifications of Laser Sources

System	A	B
Maker	Coherent	IMRA
Pulse duration	30–100fs	269fs
Repeat cycle	1kHz	200kHz
Energy/pulse	2mJ	50 μ J
Dots/sec	1,000	200,000
Average power	2W	10W

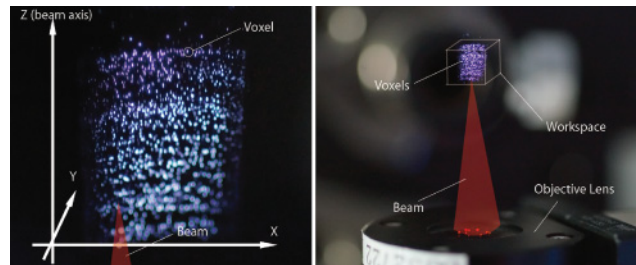


Fig. 7. Relationship between the XYZ-coordinate and the focused laser beam. Voxels are rendered above the objective lens.

The galvano mirror scans the emission dot along the lateral directions (X and Y scanning), whereas the varifocal lens can vary its focal point in the axial direction (Z scanning). The Fourier CGH is used for simultaneously addressed voxels [Hayasaki et al. 2005]. The CGH, which is designed using the ORA method, is displayed on the LCOS-SLM, which has 768×768 pixels, a pixel size of $20 \times 20\mu\text{m}^2$, and a response time of 100ms. The specifications of each component are shown in Tables III and IV. In addition to

Table III. Specifications of Galvano Mirrors

System	A	B
Maker	Canon	Intelliscan
Scan angle	± 0.17 rad	± 0.35 rad
Error	$< 5 \mu\text{rad}$	$< 5\text{mrad}$
Resolution	20 bit	20 bit

Table IV. Specifications of Varifocal Lens

System	A and B
Maker	Optotune
Aperture	10mm
Response time	$< 2.5\text{ms}$
Focal length	+45 to +120mm

these components, we use a microscope, which is connected to the computer via USB, for monitoring and recording.

4.2 Light Source

We use two light sources. The primary light source used for evaluation and application was developed by Coherent Co., Ltd., and has a center wavelength of 800nm, repetition frequency of 1kHz, and pulse energy of up to 2mJ; the pulse width is adjustable from 30 to 100fs. Figure 8 shows the spectra and pulse intensities of the 30fs and 100fs settings of this light source. Ultrashort pulses are generated by converting low-intensity and long-duration pulses to high-intensity and short-duration ones. If the time-averaged laser power is unchanged, the peak intensity differs according to the pulse width. In fact, the 30fs pulse width has a threefold greater peak intensity than the 100fs pulse width at the same time-averaged power. We refer to the system using this light source as System A.

The other light source we use is the FCPA $\mu\text{Jewel DE1050}$ from IMRA America, Inc. The laser has a center wavelength of 1,045nm, repetition frequency of 200kHz, pulse energy of up to 50 μJ , and pulse width of 269fs. We refer to the system with this light source as System B. Note that the peak intensity of the laser, rather than the pulse width, is important for producing aerial plasma. Systems A and B both have sufficient peak intensity to excite the air and generate an emission dot.

4.3 Optical Circuit

Here, we describe our optical circuit in terms of the path of the laser. Figure 6 shows the optical setup of System A. The laser is generated by the femtosecond light source and then phase-modulated by the SLM. The SLM energy conversion rate is 65% to 95%. Then, the beam spot is varied by two lenses ($F = 450$ and 150mm). This two-lens unit reduces the beam spot by a factor of 1/3. The spot is then reflected by the galvano mirror, which determines the XY position of the light. The galvano mirror and SLM are connected in an object–image correspondence. Subsequently, the beam spot is adjusted by two lenses ($F = 100$ and 150mm); this two-lens unit magnifies the beam spot 1.5-fold. Then, the light enters the varifocal lens. The varifocal lens and galvano mirror are connected in an object–image correspondence, and the former adjusts the z -axis focal points. The light enters the objective lens ($F = 40\text{mm}$). Once it exits this lens, it excites the display medium (air). The energy conversion rate of System A is 53%.

System B has the same structure but lacks an SLM. In addition, the lens sets are slightly different from those of System A. Specifically, System B has no lens before the galvano mirror, as the

varifocal lens is positioned after the galvano mirror. Then, the beam spot is adjusted by the two-lens unit ($F = 50$ and 80mm). An F20 objective lens is employed, and System B’s total energy conversion rate is 80%.

4.4 3D Scanning System

In this subsection, we describe our scanning system in detail. Figure 6 shows the galvano and varifocal lenses. We employ galvano mirrors to scan the lateral directions (X and Y scanning), while the varifocal lens can change its focal point in the beam axial direction (Z scanning). For system A, we utilize a Canon GH-315 driven by GB-501 as the galvano mirror, and for System B we employ an Intelliscan 20i to scan the beams. Both are connected by PCI boards. Table III shows the specifications of each of the galvano mirrors. As the varifocal lens for both Systems A and B, we employ an Optotune EL-10-30, which is connected via serial USB to a personal computer. The specifications of the varifocal lens are shown in Table IV. These devices are operated by original applications coded in C++.

4.5 LCSLM

The LCSLM (Hamamatsu, PPM) is a parallel-aligned nematic liquid crystal SLM (PAL-SLM) coupled with a liquid crystal display (LCD) and a 680nm laser diode (LD). This device, which can perform phase-only modulation of more than 2rad, is frequently used to display real-time CGHs. The PAL-SLM is composed of a liquid crystal (LC) layer, a dielectric mirror, and an optically addressed photoconductive (PC) layer containing amorphous silicon, which are sandwiched between two transparent indium tin oxide electrodes. The LC molecules are aligned in parallel. When incident light illuminates the PC layer, the impedance of this layer decreases, and the electric field across the LC layer increases accordingly. With this increased field, the LC molecules become tilted in the propagation direction of the readout light, and the effective refractive index of the LC layer decreases. Pure phase modulation occurs only when the polarization direction of the femtosecond laser is parallel to the aligned direction of the LC molecules. The CGH pattern on the LCD illuminated by the LD is applied to the PC layer through imaging optics.

4.6 Control System

Figure 6 shows our system diagram. The system is controlled using a personal computer running the Windows operating system, and all programs are coded in C++. The control system operates the SLM, galvano mirror, and varifocal lenses. To monitor the interaction, a USB microscope is connected to the system. The galvano and varifocal lenses run along different threads and are synchronized when new draw patterns are input. The user input is captured at 20Hz, and the SLM is connected to the computer as an external display.

5. EXPERIMENTS AND EVALUATIONS

In this section, we describe our experiments and system evaluation procedures. First, we present an overview of our experimental plan and results. Then, we report the results of the following tests: energy versus ionized plasma brightness, brightness versus pulse peak, simultaneously addressed voxels for aerial images, and skin damage. In the experiments, the brightness is measured as a summation of all the pixel values within a close-up image of the plasma taken by

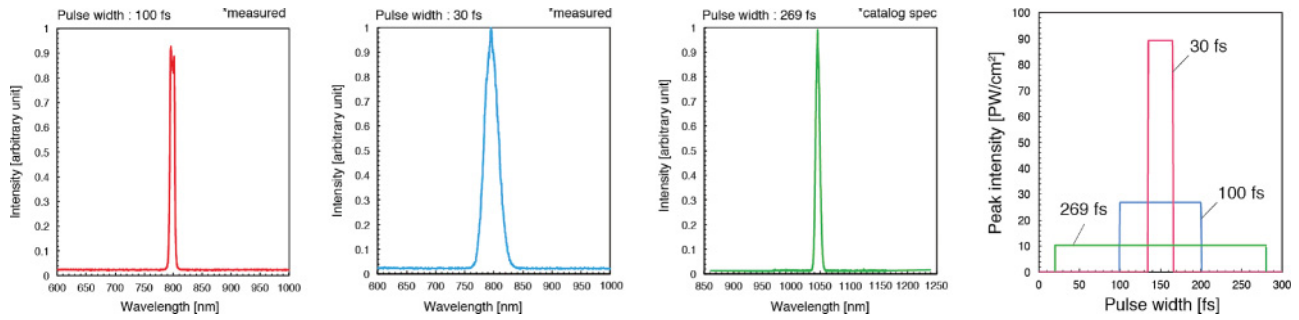


Fig. 8. Spectra of 100fs, 30fs, and 269fs lasers (from left to right). The rightmost illustrates the peak intensity and the pulse width of each femtosecond lasers.

a digital camera, which is a common definition in the field of laser optics.

We tested not only gas-ionized plasma but also photon absorption and cavitation in order to compare the various energy consumption performances and the means of applying the femtosecond laser system to display technology. All experiments were conducted using System A, which is described in Section 4.

5.1 Overview of Experiments

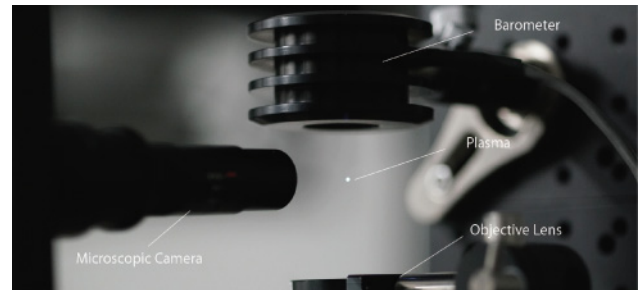
In this study, we propose a femtosecond-laser-based display system design. In previous works [Kimura et al. 2006; Saito et al. 2008], the requirements, scalability, and risks of such laser-based systems are not thoroughly discussed. There are several factors that we should explore. In Section 5.2, we examine the voxel brightness, which is important in relation to the energy and display spatiotemporal resolution, as discussed in Section 3. In Section 5.3, we explore the relationship between the pulse duration and brightness. This is important for scalability, particularly when a faster laser source is developed. In Section 5.4, we explore simultaneously addressed voxels using an SLM. This is important for scalability with regard to increasing the spatiotemporal resolution. Then, in Section 5.5, we examine risk issues and the effect of the plasma on the skin. This is important because this technology is intended for widespread general use. Finally, in Section 5.6, we examine audible sound from the plasma generated by femtosecond lasers. This is important because this technology is intended for use in everyday life.

5.2 Energy versus Brightness

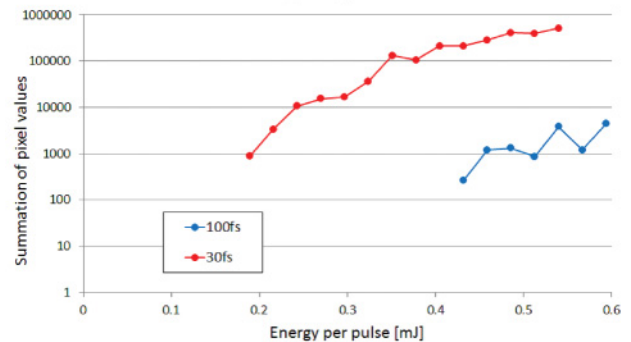
We conducted this experiment to evaluate the relationship between the plasma-production energy level and the resultant brightness of the image. This experiment aimed to confirm the feasibility of our system and to investigate how it can be applied to display voxels; thus, the minimum peak intensity value was determined.

We conducted the experiments using System A (30fs) and employed a microscope to capture the resultant image. With our setup, the laser source can provide a time-averaged power of up to 7W; however, unwanted breakdown occurs in the light path before the objective lens when the power is too high. Hence, the full power of the laser source cannot be used. Moreover, the capacity of our SLM is not guaranteed above 2W. The experiments were conducted for a time-averaged power range of 0.05 to 1.00W.

Figure 9 (30fs) shows the experimental setup and results. The experiments were conducted under energies per pulse of 0.16 to 0.55mJ. The 30fs laser can produce plasma at a pulse energy of 0.2mJ. The cross-sectional area of the focal point is theoretically calculated to be $2 \times 10^{-7} \text{cm}^2$. Then, the peak intensity is



(a) Setup.



(b) Results.

Fig. 9. Experimental setup and results on brightness of light emission in air induced by 30fs and 100fs lasers.

36PW/cm^2 , which is clearly higher than the ionized plasma threshold ($> 1 \text{PW/cm}^2$).

5.3 Brightness versus Pulse Peak

The relationship between the pulse peak and the resultant image brightness was also examined, as the peak intensity plays an important role in plasma generation. This experiment aimed to classify systems of different pulse width in terms of the display voxel brightness.

As in the previous experiment, we conducted experiments using System A (30 and 100fs). Pulses of 30 and 100fs yield different spectra and instantaneous power for the same time-averaged power. In addition, the 30fs setting yields a threefold higher peak pulse. We employed the same microscope to capture the image as that used in Section 5.1, and the results are shown in Figure 9. The experiments were conducted for a power range of 0.05 to 1.00W.

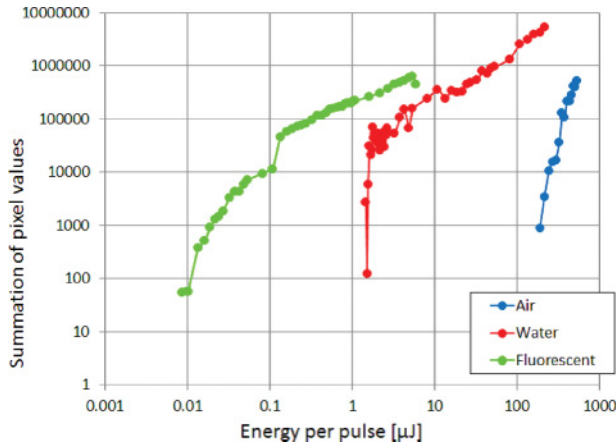


Fig. 10. Experimental results on brightness of light emission in air, water, and fluorescence solution induced by 30fs laser.

It was found that a 100fs laser can generate plasma at a pulse energy of 0.45mJ. Then, the peak intensity is 24PW/cm², which is clearly higher than the ionized plasma threshold (>1PW/cm²). Further, it is confirmed that the 30fs pulse requires less energy than the 100fs pulse to produce plasma under the same time-averaged power.

Additionally, we conducted other experiments comparing media materials (air, water, and fluorescent solution). The results are shown in Figure 10, which shows that the required pulse energy differs dramatically depending on the medium.

5.4 Simultaneously Addressed Voxels

One of the main contributions of this article is the application of an SLM to in-air laser plasma graphics. This enables simultaneously addressed voxels using CGHs. (Note that in previous works [Kimura et al. 2006; Saito et al. 2008], multiple voxels were not generated simultaneously.) Simultaneous addressing is important for increasing the spatiotemporal resolution, although the simultaneously addressed voxels are darker than a single point because the energy is distributed among them. This experiment was designed to explore the resolution scalability by using an SLM with a single light source. Simultaneous addressing can be obtained for both the lateral (X, Y) and beam (Z) axes by displaying appropriate holograms on a single SLM. Here, we investigated simultaneous addressing for the lateral axis. Again, the experiments were conducted using System A (30fs), and Figure 11 shows the results and the holographic images used in the SLM. We employed the microscope shown in Figure 9. We conducted the experiments using time-averaged laser powers from 0.05 to 1.84W. We had one to four simultaneously addressed voxels, and five or more voxels were not visible.

5.5 Skin Damage

Another main contribution of this article is an estimation of the risk of femtosecond laser systems. Plasma can be harmful to humans. However, a femtosecond pulse is an ultrashort pulse and is used for breaking without the use of heat for industrial purposes. It is also used for ultrashort-scale fabrication on the submicrometer scale.

Thus, we supposed that such pulses may not damage human skin seriously. In addition, our display scans a 3D space very rapidly; therefore, the laser spot does not remain at a specific point for a long period. On the other hand, this plasma still poses dangers

to the retina. However, we believe that the potential for general application still exists with appropriate installation.

Therefore, we conducted this experiment to explore the damage to skin structure caused by femtosecond plasma exposure. In these experiments, we employed leather as a substitute for human skin.

The experiments were conducted using System A (30fs and 1W, 100fs and 1W), and the plasma exposure duration was varied between 50 and 6,000ms. Figure 12 shows the results. It was found that the 30fs and 100fs pulses have almost the same effect on the skin. As we described above, the 30fs pulse has a threefold greater instantaneous power and can generate brighter voxels. However, 50 shots occur in 50ms, and there is almost no difference between the 30fs and 100fs results. In this experiment, the time-averaged power is the factor determining the result. For exposures of less than 2,000ms (2,000 shots), only 100 μ m-diameter holes appeared, and there was no heat damage to the leather. For a period of longer than 2,000ms, heat effects were observed around the holes.

We conducted a test with a nanosecond laser for comparison with this result. With the nanosecond laser, the leather burned within 100ms. This means that the pulse duration, repetition time, and time-averaged power are important factors affecting the level of damage caused by the laser.

Hence, this laser is sufficiently less harmful for use. Further, there are two ways to reduce the damage to the skin: using an ultrashort-pulse laser, which is bright and has a time-averaged power that is not intense, or increasing the scanning speed.

5.6 Noise Level

Laser plasma in air radiates not only visible light but also audible sound. We conducted an experiment to evaluate the radiated sound. The position of the laser plasma was fixed. The time-averaged laser power was set to 1.0 or 1.2W. The pulse width was set to 40, 60, 80, or 100fs. The noise level was measured by a noise level meter (NL-52, Rion Co., Ltd.), which was placed 20mm from the laser plasma. The background noise level was 55.7dB SPL. The brightness of the laser plasma was also recorded.

The results are shown in Figure 13. The maximum noise level was 77.2dB SPL with 40-fs pulses, which also yielded the brightest radiation. This noise level was not very subjectively annoying, and it is acceptable in everyday life. Brighter plasma emission tends to be accompanied by louder sound; 40fs pulses radiate louder sound and brighter light.

6. APPLICATIONS

In this section, we describe potential applications of our system. We introduce a 3D aerial display system and describe the interaction between the system and users (Figure 2).

6.1 Aerial Displays

In this subsection, we describe our aerial display using laser plasma. We developed our application for both Systems A and B, and the results are shown in Figures 14(a), 14(b), and 14(d). For Systems A and B, the workspaces are 10 \times 10 \times 10 and 8 \times 8 \times 8mm³, respectively. These workspaces are smaller than those in previous works [Kimura et al. 2006; Saito et al. 2008], but the resolutions are 10 to 200 times higher than those in previous works. The maximum spatiotemporal resolution is 4,000 points/s (with simultaneous addressing of four voxels) for System A and 200,000 point/s for System B. The image frame rate is determined by the number of vertices used in the image.

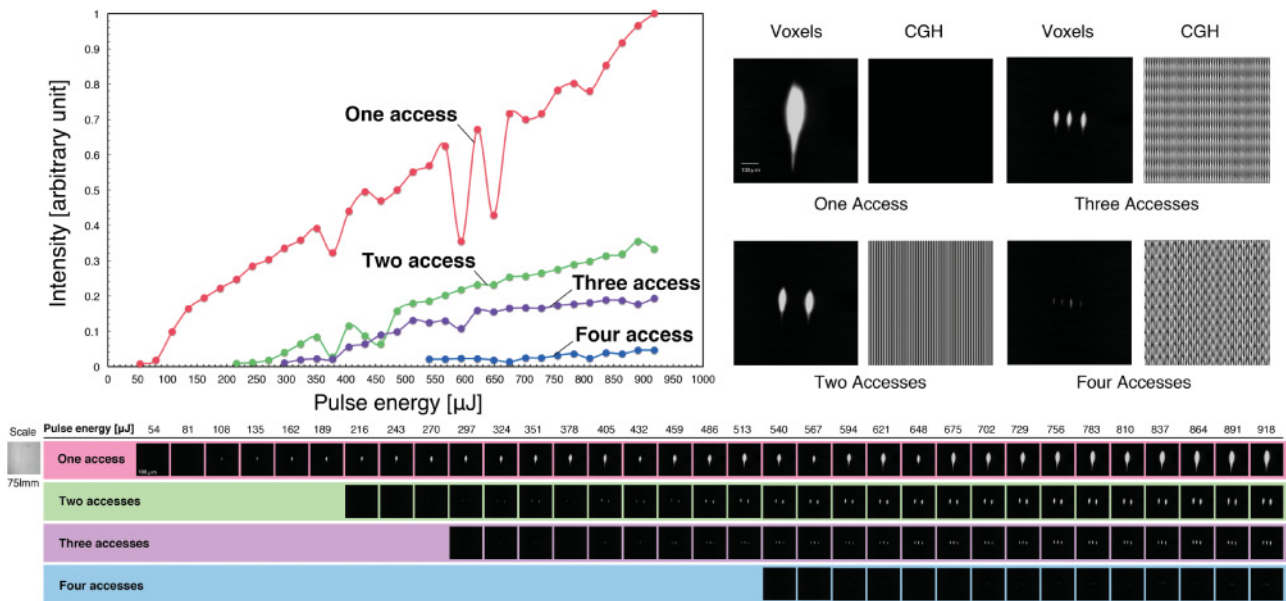


Fig. 11. Experimental results on simultaneous addressing. One to four addressing were tested. The intensity is the normalized value of the summation of all the pixel values of the photos of the voxels, which is taken a evaluative value of brightness.

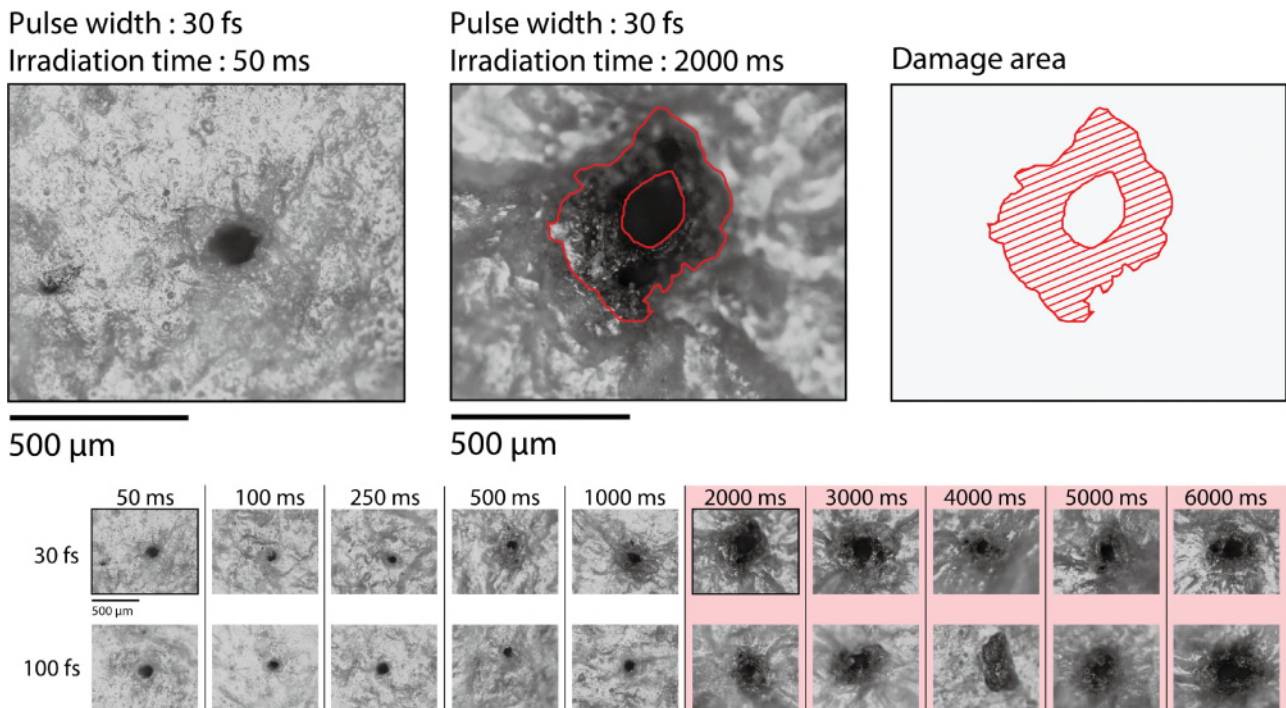


Fig. 12. Experimental results on skin damage. Leather sheets were exposed to the 30fs and 100fs lasers and the irradiation time was controlled. The exposure longer than 2,000ms burns the leather surface.

6.1.1 *Spatial AR to Real-World Object.* This aerial display can be used with real-world objects, as shown in Figures 14(e) and 14(f). One of the merits of the spatial AR to real-world object technique is that the AR content is on the same scale as the object, which is overlapped. In addition, this system was developed to include a microscope, which can detect an object in the workspace, overlap

it with the contents, and modify the contents when contact between the object and the plasma occurs.

This has an advantage over conventional AR approaches in terms of correspondence to the 3D spatial position. Digital content and information are directly provided in a 3D space instead of on a 2D computer display.

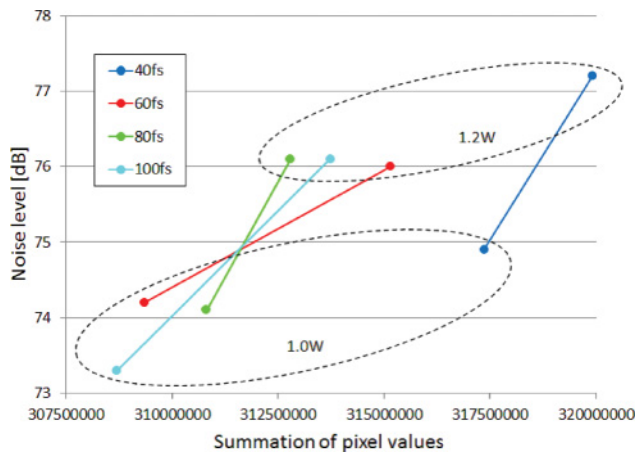


Fig. 13. Experimental results on noise level vs. brightness of light emission. The background noise level was 55.7dB SPL.

6.1.2 Aerial Interaction with Aerial Content. Our system has the unique characteristic that the plasma is touchable. It was found that contact between the plasma and a finger causes a brighter light. This effect can be used as a cue indicating contact.

Figures 14(c) and 14(g) show examples of this interaction. One possible control is touch interaction in which floating images change when touched by a user. The other is damage reduction. For safety, the plasma voxels are shut off within a single frame (17ms = 1/60s) when users touch the voxels. This is sufficiently less than the harmful exposure time (2,000ms) determined in Section 5.4.

6.1.3 Haptic Feedback on Aerial Images. Shock waves are generated by plasma when a user touches the plasma voxels. Then the user feels an impulse on the finger as if the light has physical substance. A detailed investigation of the characteristics of this plasma-generated haptic sensation with sophisticated spatiotemporal control is beyond the scope of this article.

However, example applications such as an aerial “check box” are at least expected. Figure 14 shows the interaction between the user and the aerial image.

7. DISCUSSION

7.1 Laser-Induced Emission Phenomena

There are two laser-induced emission phenomena other than plasma emission: fluorescence and diffusion by cavitation, as mentioned in Section 3.1. Both can be applied to displays using the laser-and-SLM system. In this section, the differences between the emission phenomena are explained.

The display medium is the key factor determining the potential interactions. Whereas plasma is generated in air, fluorescence requires fluorescent materials (e.g., ink or pigment), and cavitation requires a fluid medium. The medium also determines the power that is required for light emission. The order of the required power decreases from air (petawatts per centimeter squared) to water to fluorescent materials (megawatts per centimeter squared).

The available wavelengths also differ in these cases. The plasma color is wavelength-independent; hence, it is reasonable to use invisible wavelengths (e.g., infrared or ultraviolet). For fluorescence, multielectron fluorescence is reasonable; in this case, multiple photons are absorbed by molecules, and a single photon with a shorter wavelength is emitted. Full-color rendering is possible by

using multiple fluorescent materials. This is acceptable because the invisible ultraviolet source leaves only the emission visible. On the other hand, when cavitation in water is applied, a visible wavelength should be used, because the incoming wavelength is diffused by microbubbles and observed. This feature leads to full-color rendering with multiple lasers of different colors.

The softness of the medium determines the possible forms of interaction. With aerial plasma in air, users can insert their hands into the workspace and touch the plasma. This is also possible with nonfluorescent or fluorescent liquid media. However, for a fluorescent solid medium, the voxels cannot be touched directly.

7.2 Drawbacks and Limitations

An SLM is not resistant to an intense laser because its reflectance efficiency is not 100%. We cannot use the maximum time-averaged laser power, and the reflected light is also decreased. However, we are optimistic that improvement of the reflectance efficiency of SLMs will relax this limitation in future. Then greater numbers of simultaneously addressed voxels can be generated.

In addition, the optical circuit should be developed and treated carefully. Because our system utilizes high-intensity lasers, ionization may occur along the optical circuit. This also limits the available laser power so that damage to optical components is avoided. Further, plasma generation is a nonlinear phenomenon, and careful handling is required. These issues should be considered well to ensure safety.

In addition, focusing and aberration are limitations of our systems. We have to focus the light to make focal points to generate aerial plasma. Thus, the aperture of the objective lens determines the maximum workspace, which limits the angle range of the galvano mirror. In addition, high-speed variation of the varifocal lens would cause an aberration problem. The characteristics of these lenses are important in development of the optical circuit.

7.3 Scalability

7.3.1 Size of Workspace. A scalable workspace size is a main concern of our project. Aerial plasma is limited mainly by the objective lens after the varifocal lens. Laser plasma generation requires an instantaneous laser power of petawatts per centimeter squared, and an objective lens is required for this purpose. An objective lens with a larger aperture allows a larger angle range of the galvano mirror (i.e., XY scanning).

The instantaneous laser power required to excite fluorescence and microbubbles in water is small compared to that required for laser plasma, and an objective lens is not required. Thus, these workspaces are limited by the angle range of the galvano mirror and the depth range of the varifocal lens.

7.3.2 Voxels Per Second. The spatiotemporal rendering ability (voxels per second) is determined by the number of voxels simultaneously addressed by the SLM, the refresh rate of the SLM, the scanning speed of the galvano mirror, and the response time of the varifocal lens. The galvano mirror is the fastest (more than 1kHz), and the other components work at less than 100Hz. It is hence reasonable to use mainly the galvano mirror. In addition, the SLM can render up to four points simultaneously. Then the four voxels are moved together by galvano scanning, and 4,000 dots/s is achieved. Although the use of the SLM increases the cost and complexity of the optical circuit, the multiplication of voxels is a considerable benefit.

We have to develop three factors to scale up our system for everyday applications: increasing the time-averaged power of the

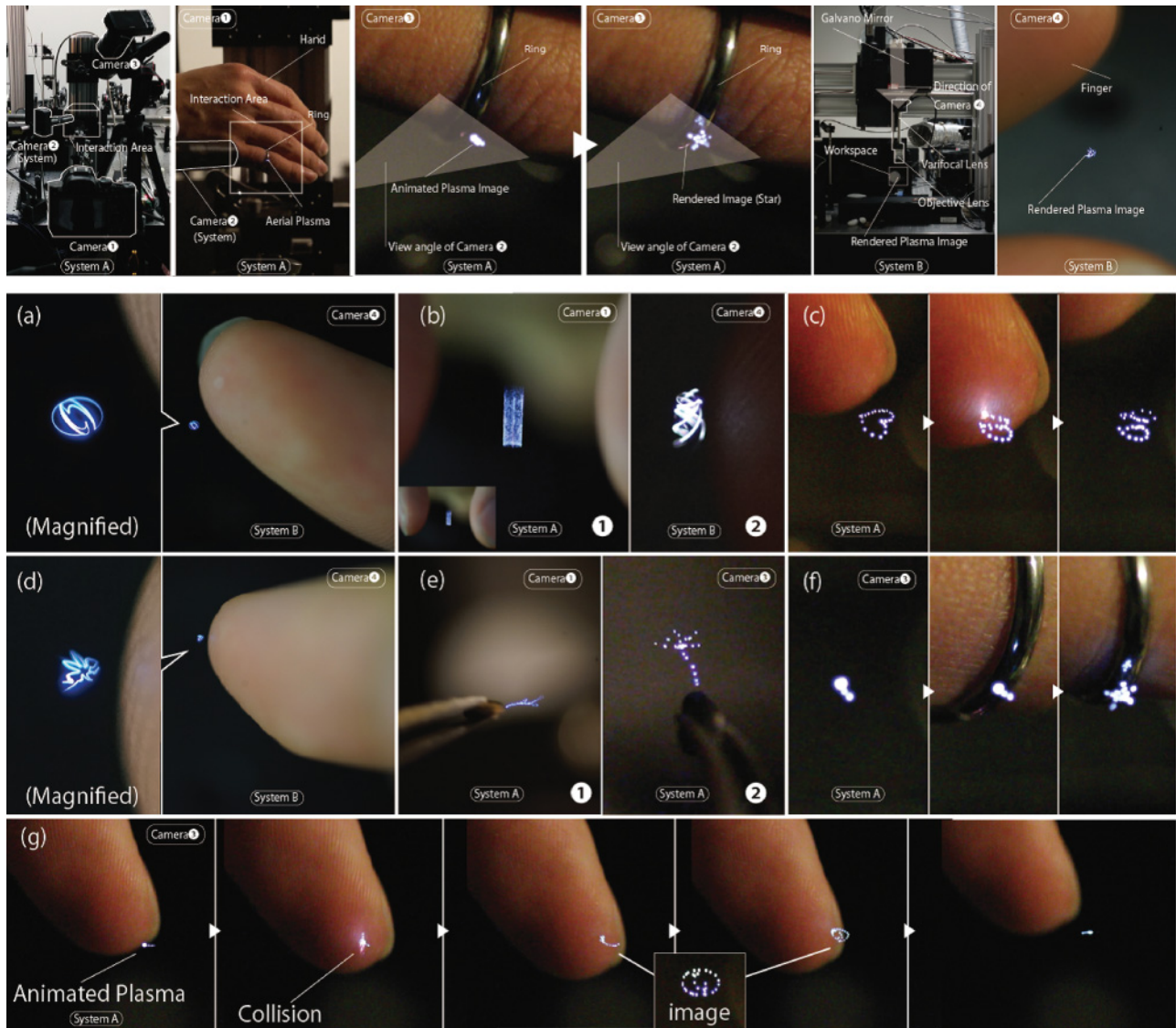


Fig. 14. Results of aerial rendering. (Uppermost) The setups of Systems A and B. (a) The SIGGRAPH logo, (b) a cylinder, (c) a “heart” that is broken by touch, (d) a “fairy,” (e) “sprouts” coming out from seeds, (f) a light point that changes into a “jewel” in contact with a ring, and (g) direct interaction between a light point and a finger.

laser source, shortening the pulse width to increase the instantaneous power, and increasing the scanning speed. These factors enable us to have a number of simultaneously addressed and scanned voxels within a single frame, maintaining the features of visibility and touchability.

A higher time-averaged laser power yields more simultaneously addressed voxels. The laser power is limited by the damage to the skin, unwanted ionization along the optical circuit, and the reflection/transmission characteristics of the optical devices.

Shortening the pulse width has two benefits. One is a higher repetition frequency (i.e., more dots per second), which maintains the high instantaneous power required for plasma generation. The other is reduced harmfulness to human skin because of the lower amount of pulse energy with a fixed instantaneous power.

There is little room to improve the scanning speed of the galvano mirror and varifocal lens. Employing multiple laser systems is one of the solutions for generating multiple voxels.

7.4 Risk of Laser

Class 4 laser sources are used in this article. The proposed display system was carefully designed and operated on the basis of International Electrotechnical Commission (IEC) 60825-1:2014. There are two concerns regarding the risk of lasers: damage to the eyes and to the skin.

Direct viewing of the laser beam by users should be avoided. Because the laser plasma emits visible light in all directions at the focal point, users can see it from the side of the laser beam. It is still

recommended that users wear glasses with infrared filters until this display technology is mature.

There are a few reports on damage to the skin by femtosecond lasers. The minimum visible lesion thresholds for porcine skin for pulsed lasers were evaluated in Cain et al. [2007]. The ED₅₀ for a femtosecond laser (44fs, 810nm, and 12mm spot size) was determined to be 21mJ from the observation that the lesions produced by lasers with less than that energy value disappeared at 24 hours after exposure. The energy (2mJ and 50μJ for lasers A and B, respectively) and spot size (<10 μm) are much smaller, and we expect that damage by these femtosecond lasers is negligible. We also investigated the exposure time in this article. The result shows that there was a discontinuous expansion of the damaged area when the exposure time reached 2,000ms. We can minimize the damage by keeping the exposure time below 2,000ms by, for example, feedback control based on the detection of brighter plasma emission at the surface of the finger in contact with the aerial laser plasma.

8. CONCLUSION

In this article, we introduced a system for rendering volumetric graphics in air using a femtosecond laser. Aerial laser-induced plasma emits light without interaction with any special materials, and one advantage of the femtosecond-laser display system is that it is less harmful to the skin than a system using a nanosecond laser.

There are two methods of rendering graphics in air with a femtosecond laser: producing holograms by SLM technology and scanning of a laser beam by a galvano mirror. The hologram size and workspace of the current system have maximum values of 1cm² and 5cm³, respectively. Although these demonstrated sizes are currently too small for use in the applications shown in Figure 2, this study is the first step in discussing and designing laser-based aerial volumetric displays. These sizes are scalable depending on the optical devices and setup.

This paper reports the details of the theoretical principles, system setup, and experimental evaluations, and also discusses the system's scalability, limitations, and applications. Although we focus on laser-induced plasma, the same considerations can be applied to other emission techniques such as fluorescence and cavitation.

REFERENCES

- M. V. Ammosov, N. B. Delone, and V. P. Krainov. 1986. Tunnel ionization of complex atoms and of atomic ions in an alternating electromagnetic field. *Soviet Physics - JETP* 64, 6 (1986), 1191–1194.
- Peter C. Barnum, Srinivasa G. Narasimhan, and Takeo Kanade. 2010. A Multi-layered display with water drops. *ACM Trans. Graph.* 29, 4 (July 2010), Article 76, 7 pages. DOI: <http://dx.doi.org/10.1145/1778765.1778813>
- Jörgen Bengtsson. 1994. Kinoform design with an optimal-rotation-angle method. *Appl. Opt.* 33, 29 (Oct. 1994), 6879–6884. DOI: <http://dx.doi.org/10.1364/AO.33.006879>
- P. Benzie, J. Watson, P. Surman, I. Rakkolainen, K. Hopf, H. Urey, V. Sainov, and C. von Kopylow. 2007. A survey of 3DTV displays: Techniques and technologies. *IEEE Transactions on Circuits and Systems for Video Technology* 17, 11 (Nov. 2007), 1647–1658. DOI: <http://dx.doi.org/10.1109/TCSVT.2007.905377>
- Clarence P. Cain, William P. Roach, David J. Stolarski, Gary D. Noojin, Semih S. Kumru, Kevin L. Stockton, Justin J. Zohner, and Benjamin A. Rockwell. 2007. Infrared laser damage thresholds for skin at wavelengths from 0.810 to 1.54 microns for femto-to-microsecond pulse durations. In *Proceedings of SPIE*, Vol. 6435. 64350W–64350W–12. DOI: <http://dx.doi.org/10.1117/12.715199>
- James Clar. 2008. Traffic. Retrieved from <http://www.viatraffic.org/index.php?page=3d-display-cube-v4>.
- Elizabeth Downing, Lambertus Hesselink, John Ralston, and Roger Macfarlane. 1996. A three-color, solid-state, three-dimensional display. *Science* 273, 5279 (1996), 1185–1189. DOI: <http://dx.doi.org/10.1126/science.273.5279.1185>
- S. Eitoku, T. Tanikawa, and Y. Suzuki. 2006. Display composed of water drops for filling space with materialized virtual three-dimensional objects. In *Proceedings of the 2006 Virtual Reality Conference*. 159–166. DOI: <http://dx.doi.org/10.1109/NR.2006.51>
- Gregg E. Favalora, Joshua Napoli, Deirdre M. Hall, Rick K. Dorval, Michael Giovinco, Michael J. Richmond, and Won S. Chun. 2002. 100-million-voxel volumetric display. In *Proceedings of SPIE*, Vol. 4712. 300–312. DOI: <http://dx.doi.org/10.1117/12.480930>
- Sean Follmer, Daniel Leithinger, Alex Olwal, Akimitsu Hogge, and Hiroshi Ishii. 2013. inFORM: Dynamic physical affordances and constraints through shape and object actuation. In *Proceedings of the 26th Annual ACM Symposium on User Interface Software and Technology (UIST'13)*. ACM, New York, NY, 417–426. DOI: <http://dx.doi.org/10.1145/2501988.2502032>
- Tovi Grossman and Ravin Balakrishnan. 2006. The design and evaluation of selection techniques for 3D volumetric displays. In *Proceedings of the 19th Annual ACM Symposium on User Interface Software and Technology (UIST'06)*. ACM, New York, NY, 3–12. DOI: <http://dx.doi.org/10.1145/1166253.1166257>
- Satoshi Hasegawa and Yoshio Hayasaki. 2013. Liquid volumetric display with parallel optical access by computer-generated hologram. In *Digital Holography and Three-Dimensional Imaging (2013)*, DTh2A.7. DOI: <http://dx.doi.org/10.1364/DH.2013.DTh2A.7>
- Tomoko Hashida, Yasuaki Kakehi, and Takeshi Naemura. 2011. Photochromic sculpture: Volumetric color-forming pixels. In *ACM SIGGRAPH 2011 Emerging Technologies (SIGGRAPH'11)*. ACM, New York, NY, Article 11, 1 page. DOI: <http://dx.doi.org/10.1145/2048259.2048270>
- Y. Hayasaki, T. Sugimoto, A. Takita, and N. Nishida. 2005. Variable holographic femtosecond laser processing by use of a spatial light modulator. *Applied Physics Letters* 87, 3 (2005), 031101.
- Takayuki Hoshi, Masafumi Takahashi, Kei Nakatsuma, and Hiroyuki Shinoda. 2009. Touchable holography. In *ACM SIGGRAPH 2009 Emerging Technologies (SIGGRAPH'09)*. ACM, New York, NY, Article 23, 1 pages. DOI: <http://dx.doi.org/10.1145/1597956.1597979>
- H. Ishikawa and H. Saito. 2008a. Closed-line based representation of 3D shape for point cloud for laser plasma scanning 3D display. In *Proceedings of the 18th International Conference on Artificial Reality and Telexistence (ICAT'08)*. 28–35.
- H. Ishikawa and H. Saito. 2008b. Point cloud representation of 3D shape for laser-plasma scanning 3D display. In *Proceedings of the 34th Annual IEEE Conference on Industrial Electronics (IECON'08)*. 1913–1918. DOI: <http://dx.doi.org/10.1109/IECON.2008.4758248>
- Hiroyo Ishikawa, Hayato Watanabe, Satoshi Aoki, Hideo Saito, Satoru Shimada, Masayuki Kakehata, Yuji Tsukada, and Hidei Kimura. 2011. Surface representation of 3D object for aerial 3D display. In *Proceedings of SPIE*, Vol. 7863. 78630X–78630X–8. DOI: <http://dx.doi.org/10.1117/12.872397>
- Hiroo Iwata, Hiroaki Yano, Fumitaka Nakaizumi, and Ryo Kawamura. 2001. Project FEELEX: Adding haptic surface to graphics. In *Proceedings of the 28th Annual Conference on Computer Graphics and*

- Interactive Techniques (SIGGRAPH'01)*. ACM, New York, NY, 469–476. DOI : <http://dx.doi.org/10.1145/383259.383314>
- D. G. Jansson and E. P. Berlin. 1979. A three-dimensional computer display. In *Proceedings of the 1st Annual Conference of Computer Graphics in CAD/ CAM System, 1979*.
- Andrew Jones, Ian McDowall, Hideshi Yamada, Mark Bolas, and Paul Debevec. 2007. Rendering for an interactive 360° light field display. *ACM Transactions on Graphics* 26, 3 (July 2007), Article 40. DOI : <http://dx.doi.org/10.1145/1276377.1276427>
- Abhijit Karnik, Archie Henderson, Andrew Dean, Howard Pang, Thomas Campbell, Satoshi Sakurai, Guido Herrmann, Shahram Izadi, Yoshifumi Kitamura, and Sriram Subramanian. 2011. VORTEX: Design and implementation of an interactive volumetric display. In *CHI'11 Extended Abstracts on Human Factors in Computing Systems (CHI EA'11)*. ACM, New York, NY, 2017–2022. DOI : <http://dx.doi.org/10.1145/1979742.1979870>
- L. V. Keldysh. 1965. Ionization in the field of a strong electromagnetic wave. *Soviet Physics JETP* 20 (May 1965), 1307–1314.
- Hidei Kimura, Akira Asano, Issei Fujishiro, Ayaka Nakatani, and Hayato Watanabe. 2011. True 3D display. In *ACM SIGGRAPH 2011 Emerging Technologies (SIGGRAPH'11)*. ACM, New York, NY, Article 20, 1 page. DOI : <http://dx.doi.org/10.1145/2048259.2048279>
- Hidei Kimura, Taro Uchiyama, and Hiroyuki Yoshikawa. 2006. Laser produced 3D display in the air. In *ACM SIGGRAPH 2006 Emerging Technologies (SIGGRAPH'06)*. ACM, New York, NY, Article 20. DOI : <http://dx.doi.org/10.1145/1179133.1179154>
- Cha Lee, Stephen DiVerdi, and Tobias Hollerer. 2009. Depth-fused 3D imagery on an immaterial display. *IEEE Transactions on Visualization and Computer Graphics* 15, 1 (2009), 20–33.
- Jinha Lee, Rehmi Post, and Hiroshi Ishii. 2011. ZeroN: Mid-air tangible interaction enabled by computer controlled magnetic levitation. In *Proceedings of the 24th Annual ACM Symposium on User Interface Software and Technology (UIST'11)*. ACM, New York, NY, 327–336. DOI : <http://dx.doi.org/10.1145/2047196.2047239>
- D. L. Macfarlane. 1994. Volumetric three-dimensional display. *Applied Optics* 33, 31 (Nov. 1994), 7453–7457.
- Belen Masia, Gordon Wetzstein, Piotr Didyk, and Diego Gutierrez. 2013. A survey on computational displays: Pushing the boundaries of optics, computation, and perception. *Computers & Graphics* 37, 8 (2013), 1012–1038. DOI : <http://dx.doi.org/10.1016/j.cag.2013.10.003>
- Yasushi Matoba, Taro Tokui, Ryo Sato, Toshiki Sato, and Hideki Koike. 2012. SplashDisplay: Volumetric projection using projectile beads. In *ACM SIGGRAPH 2012 Emerging Technologies (SIGGRAPH'12)*. ACM, New York, NY, Article 19, 1 page. DOI : <http://dx.doi.org/10.1145/2343456.2343475>
- Y. Ochiai, T. Hoshi, A. Oyama, and J. Rekimoto. 2013. Poppable display: A display that enables popping, breaking, and tearing interactions with people. In *Proceedings of the 2013 IEEE 2nd Global Conference on Consumer Electronics (GCCE'13)*. 124–128. DOI : <http://dx.doi.org/10.1109/GCCE.2013.6664771>
- Yoichi Ochiai, Takayuki Hoshi, and Jun Rekimoto. 2014. Pixie dust: Graphics generated by levitated and animated objects in computational acoustic-potential field. *ACM Transactions on Graphics* 33, 4 (July 2014), Article 85, 13 pages. DOI : <http://dx.doi.org/10.1145/2601097.2601118>
- E. Parker. 1948. Three-dimensional cathode-ray tube displays. *Journal of the Institution of Electrical Engineers - Part III: Radio and Communication Engineering* 95, 37 (September 1948), 371–387.
- Thiago Pereira, Szymon Rusinkiewicz, and Wojciech Matusik. 2014. Computational light routing: 3D printed optical fibers for sensing and display. *ACM Transactions on Graphics* 33, 3 (June 2014), Article 24, 13 pages. DOI : <http://dx.doi.org/10.1145/2602140>
- K. Perlin and J. Y. Han. 2006. Volumetric display with dust as the participating medium. (Feb. 14 2006). Retrieved from <https://www.google.com/patents/US6997558> US Patent 6, 997, 558.
- Ivan Poupyrev, Tatsushi Nashida, Shigeaki Maruyama, Jun Rekimoto, and Yasufumi Yamaji. 2004. Lumen: Interactive visual and shape display for calm computing. In *ACM SIGGRAPH 2004 Emerging Technologies (SIGGRAPH'04)*. ACM, New York, NY, 17. DOI : <http://dx.doi.org/10.1145/1186155.1186173>
- Ismo Rakkolainen, Stephen DiVerdi, Alex Olwal, Nicola Candussi, Tobias Hüllerer, Markku Laitinen, Mika Piirto, and Karri Palovuori. 2005a. The interactive fogscreen. In *ACM SIGGRAPH 2005 Emerging Technologies (SIGGRAPH'05)*. ACM, New York, NY, Article 8. DOI : <http://dx.doi.org/10.1145/1187297.1187306>
- Ismo Rakkolainen, Stephen DiVerdi, Alex Olwal, Nicola Candussi, Tobias Hüllerer, Markku Laitinen, Mika Piirto, and Karri Palovuori. 2005b. The interactive fogscreen. In *ACM SIGGRAPH 2005 Emerging Technologies (SIGGRAPH'05)*. ACM, New York, NY, Article 8. DOI : <http://dx.doi.org/10.1145/1187297.1187306>
- Hideo Saito, Hidei Kimura, Satoru Shimada, Takeshi Naemura, Jun Kayahara, Songkran Jarusirisawad, Vincent Nozick, Hiroyo Ishikawa, Toshiyuki Murakami, Jun Aoki, Akira Asano, Tatsumi Kimura, Masayuki Kakehata, Fumio Sasaki, Hidehiko Yashiro, Masahiko Mori, Kenji Torizuka, and Kouta Ino. 2008. Laser-plasma scanning 3D display for putting digital contents in free space. In *Proceedings of SPIE* 6803 (2008), 680309–680309–10. DOI : <http://dx.doi.org/10.1117/12.768068>
- Parviz Soltan, John A. Trias, Waldo R. Robinson, and Weldon J. Dahlke. 1992. Laser-based 3-D volumetric display system. In *Proceedings of SPIE*, Vol. 1664. 177–192. DOI : <http://dx.doi.org/10.1117/12.60362>
- Alan Sullivan. 2004. DepthCube solid-state 3D volumetric display. In *Proceedings of SPIE*, Vol. 5291. 279–284. DOI : <http://dx.doi.org/10.1117/12.527543>
- Ivan E. Sutherland. 1968. A head-mounted three dimensional display. In *Proceedings of the December 9-11, 1968, Fall Joint Computer Conference, Part 1 (AFIPS'68 (Fall, part 1))*. ACM, New York, NY, 757–764. DOI : <http://dx.doi.org/10.1145/1476589.1476686>
- Karl Willis, Eric Brockmeyer, Scott Hudson, and Ivan Poupyrev. 2012. Printed optics: 3D printing of embedded optical elements for interactive devices. In *Proceedings of the 25th Annual ACM Symposium on User Interface Software and Technology (UIST'12)*. ACM, New York, NY, 589–598. DOI : <http://dx.doi.org/10.1145/2380116.2380190>
- Takumi Yoshida, Sho Kamuro, Kouta Minamizawa, Hideaki Nii, and Susumu Tachi. 2010. RePro3D: Full-parallax 3D display using retro-reflective projection technology. In *ACM SIGGRAPH 2010 Emerging Technologies (SIGGRAPH'10)*. ACM, New York, NY, Article 20, 1 page. DOI : <http://dx.doi.org/10.1145/1836821.1836841>

Received June 2015; revised November 2015; accepted November 2015